



In situ determination of atmospheric aerosol composition as a function of hygroscopic growth

Hanna Herich,¹ Lukas Kammermann,² Martin Gysel,² Ernest Weingartner,²
Urs Baltensperger,² Ulrike Lohmann,¹ and Daniel J. Cziczo^{1,3}

Received 11 February 2008; revised 1 April 2008; accepted 15 May 2008; published 30 August 2008.

[1] An in situ measurement setup to determine the chemical composition of aerosols as a function of hygroscopicity is presented. This has been done by connecting a custom-built Hygroscopicity Tandem Differential Mobility Analyzer (HTDMA) and an Aerosol Time-of-Flight Mass Spectrometer (ATOFMS), commercially available from TSI (Model 3800). Single particle bipolar mass spectra from aerosols leaving the HTDMA could thus be obtained as a function of the hygroscopic growth factor. For these studies the HTDMA was set at a relative humidity of 82% and particles with a dry diameter of 260 nm were selected. The setup was first laboratory tested, after which field experiments were performed. Two data sets were obtained during wintertime 2007 in Switzerland: the first in the urban Zurich environment and the other at the remote high alpine research station Jungfraujoch (JFJ). In Zurich, several thousand mass spectra were obtained in less than 2 days of sampling due to a high aerosol loading. At the JFJ, due to low particle concentrations in free tropospheric air masses, a longer sampling period was required. Both in Zurich and at the JFJ, two different growth factor modes were observed. Results from these two locations show that most aerosol particles were a mixture of several compounds. A large contribution of organics and combustion species was found in the less hygroscopic growth mode for both locations. Noncombustion refractory material (e.g., metals, mineral dust, and fly ash) was also highly enhanced in the nonhygroscopic particles. Sulfate, normally considered highly soluble, was found to be a constituent in almost all particles independent of their hygroscopic growth factor.

Citation: Herich, H., L. Kammermann, M. Gysel, E. Weingartner, U. Baltensperger, U. Lohmann, and D. J. Cziczo (2008), In situ determination of atmospheric aerosol composition as a function of hygroscopic growth, *J. Geophys. Res.*, *113*, D16213, doi:10.1029/2008JD009954.

1. Introduction

[2] Atmospheric aerosols, both natural and anthropogenic, have an important effect on climate forcing. The forcing can be split into a direct [McCormick and Ludwig, 1967; Charlson and Pilat, 1969] and an indirect component [Twomey, 1977; Rosenfeld and Lensky, 1998; Lohmann and Feichter, 2005]. Scattering and absorption of incoming and outgoing radiation are direct effects. Some aerosol particles have the ability to act as cloud condensation nuclei (CCN). Changes in aerosols can therefore lead to changes in cloud properties and these are considered indirect effects. Both aerosol effects are known to have a net negative contribution to the Earth's radiative forcing but the magnitude is highly uncertain [IPCC, 2007].

[3] An understanding of the direct effect requires an understanding of the ambient aerosol [Nenes *et al.*, 2002]. For example, it is well known that particles consisting of hygroscopic compounds (e.g., inorganic salts) grow and form solution droplets at a composition-dependent relative humidity (RH) whereas particles consisting of hydrophobic material (e.g., fresh soot) do not grow significantly under the same conditions. Likewise, the indirect effect is inherently related to ambient aerosol properties. Of these, aerosol size and chemical composition are the principal properties determining CCN formation. While aerosol size alone has been found to be an important determinant for CCN activation [Dusek *et al.*, 2006], chemistry also affects the ability of an aerosol to take up water [Baltensperger *et al.*, 2002; Hegg *et al.*, 2006].

[4] There are also reasons to understand the coupling between aerosol chemistry and hygroscopic growth beyond climate. One example is the effect of aerosol phase on heterogeneous chemistry. It is known that the N₂O₅ hydrolysis reaction only proceeds quickly on aqueous particles [Mozurkewich and Calvert, 1988; Hu and Abbatt, 1997]. To date our knowledge of the relationship between atmospheric aerosol chemical composition and hygroscopic growth remains limited.

¹Institute for Atmospheric and Climate Science, ETH Zurich, Zurich, Switzerland.

²Laboratory of Atmospheric Chemistry, Paul Scherrer Institut, Villigen, Switzerland.

³Now at Atmospheric Science and Global Change, Pacific Northwest National Laboratory, Richland, Washington, USA.

[5] Water uptake of aerosol particles at RH below about 95% is commonly determined with a Hygroscopicity Tandem Differential Mobility Analyzer (HTDMA) [Rader *et al.*, 1987; Brechtel and Kreidenweis, 2000a, 2000b; Weingartner *et al.*, 2002]. The hygroscopic growth factor (GF) is a common quantity for the water uptake of an aerosol particle at a certain RH which can be obtained with a HTDMA. GF is defined as:

$$GF(RH) = D_{RH}/D_0 \quad (1)$$

where D_{RH} is the particle diameter at a certain RH, D_0 is the dry size of the particle, theoretically the diameter at 0% RH. In practice, an actual humidity this low is not attainable in a HTDMA; a typical value in our setup was 10–20%. HTDMAs have been deployed in several field campaigns around the globe (summarized by Chan and Chan [2005] and E. Swietlicki *et al.*, Hygroscopic properties of sub-micrometer atmospheric aerosol particles measured with HTDMA instruments in various environments - A review, submitted to Tellus B., 2008). Bimodal or even multimodal GFs have often been found for a single air mass.

[6] The typical output of a HTDMA is a growth factor probability distribution at a given RH. This is accomplished by passing the output of the second of the DMAs to a condensation particle counter (CPC) which provides a particle number density as a function of selected D_0 and GF(RH). More recently, researchers have attempted to connect an additional measurement device to the HTDMA output. Specifically, instruments that are able to determine the chemical composition of particles have been utilized. For example, a traditional impactor with a sampling interval of 24 hours was used by Pitchford and McMurry [1994]. The samples were analyzed with X-ray fluorescence and ion chromatography. In later studies electron microscopy (EM) was used by McMurry *et al.* [1996] but the role of internally and externally mixed aerosols and hygroscopicity could not be distinguished. In neither of these cases could the aerosol composition be obtained in real time. Buzorius *et al.* [2002] deployed a Single Particle Laser Ablation Time-of-Fight Mass Spectrometer (SPLAT-MS) to analyze HTDMA data. Thus hygroscopicity and composition could be determined simultaneously. The authors used this technique in the laboratory and showed that polystyrene latex (PSL) spheres coated with ammonium nitrate had hygroscopic properties that depended on the coating thickness. Mass spectral features (i.e., the presence and abundance of specific ions) correlated with the growth factor. Besides the laboratory data field data from a single location was presented.

[7] Here we present a new setup designed and built in order to perform real-time in situ measurements of aerosol chemical composition as a function of hygroscopic growth. A HTDMA, based on the instrument described by Weingartner *et al.* [2002] at the Paul Scherrer Institute (PSI) according to directives developed within the European Commission project EUSAAR (European Supersites for Atmospheric Aerosol Research), was used for particle humidification and segregation. Particle chemical composition, in the form of bipolar single particle mass spectra, was determined with an Aerosol Time-of-Flight Mass Spectrometer (ATOFMS), commercially available from TSI (Model 3800, TSI Inc., MN). Proof of concept studies were performed with sodium

nitrate (NaNO_3) coated PSL spheres, analogous to the method of Buzorius *et al.* [2002]. Subsequent results from two field studies are presented. The first field experiment was performed at the Swiss Federal Institute of Technology (ETH) in the urban Zurich environment and the second at the remote high alpine research station Jungfraujoch (JFJ).

2. Experimental Procedure

2.1. Measurement Setup

[8] The experimental setup used in these studies is illustrated schematically in Figure 1. An aerosol flow is initially dried in a Nafion dryer to $\sim 20\%$ RH and sent to a krypton-85 neutralizer. The charged particles enter the HTDMA system which consists of two differential mobility analyzers (DMAs) separated by a humidification section. Both DMAs were custom-built by PSI based on the TSI 3071 column. With DMA1 a narrow size range is selected out of the polydisperse aerosol distribution. The monodisperse output, defined as the mobility diameter D_0 , is then humidified. The humidity is kept constant through DMA2 where it is monitored and controlled with a dew point sensor. It is important to note that the entire HTDMA setup is placed in a cooled water bath with a temperature of typically 5°C below the lab temperature. Assuming a relative temperature accuracy of $\pm 0.02^\circ\text{C}$ between the temperature and dewpoint probes the isothermal nature allows the accuracy for RH in the second DMA to remain below 1.2% at 90% RH. The residence time of the aerosol in humidified conditions is approximately 15 s. The humidified aerosol passes to DMA2 and then to a CPC and an ATOFMS. The ATOFMS had a flow rate of 0.1 l/min. In Zurich a CPC with a flow rate of 0.3 l/min (TSI, Model 3022A) was used while at the JFJ a CPC with a flow rate of 1 l/min (TSI, Model 3010) was used. In the latter case the flow was diluted with 0.7 l/min filtered air to have flow conditions in the HTDMA equivalent to those in Zurich. Capillaries are used for the aerosol transport to the CPC and ATOFMS to ensure minimal delay times (~ 10 seconds). DMA2 operates in a scanning mode to observe particle size changes due to humidification. In this manner particle concentrations after the TDMA as a function of growth factor are determined with the CPC while the chemical composition of single particles is simultaneously determined with the ATOFMS.

[9] The ATOFMS is a single particle mass spectrometer described in detail by Gard *et al.* [1997]. A brief description follows. Particles are focused into the instrument with an aerodynamic lens. Particles are accelerated such that their velocity is a function of their aerodynamic diameter. After passing two pumping stages this velocity is determined in a sizing region. The particles pass two neodymium-doped yttrium aluminum garnet (Nd:YAG) sizing lasers ($\lambda = 532$ nm) which are set at a known distance apart from each other. The scattering signals of the lasers are detected with two photomultipliers and this allows for a calculation of the flight velocity. Light scattering intensity sets a lower size limit of approximately 200 nm (i.e., particles smaller than this size scatter insufficient light to create a detectable signal at the photomultipliers) although transmission begins to fall off below 300 nm. Light scattering is known to be a function of the specific aerosol

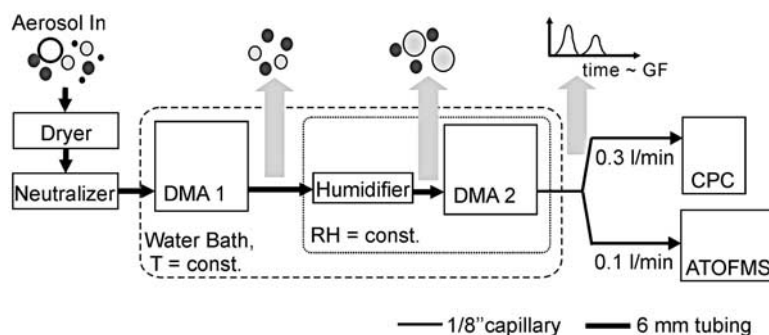


Figure 1. Experimental setup schematic. With DMA1 of a HTDMA incoming dry aerosols are size segregated and then humidified. The size distribution after humidification is monitored in scans from DMA2 with a CPC. In parallel single-particle mass spectra of the exiting particles are obtained with an ATOFMS. Shaded spheres represent aerosol composition, and size represents growth factor. Two hypothetical aerosol types with different growth factors are transmitted through DMA1 in this example.

material. Aerodynamic focusing falls off above ~ 600 nm with no particles larger than 3 micrometers observed during these studies [Liu *et al.*, 1995a, 1995b]. The particles then pass into the mass spectrometer region where the calculated flight velocity is used to trigger the firing of a desorption and ionization laser (fourth harmonic Nd:YAG, $\lambda = 266$ nm). Both the ablation and ionization processes are dependant on the specific material properties. The generated ions, depending on their polarity, are accelerated into one of two time-of-flight tubes. Positive and negative mass spectra are thus obtained simultaneously and in real time from a single particle. During the last decade ATOFMS instruments have been deployed in several field studies [e.g., Gard *et al.*, 1998; Sullivan and Prather, 2005; Gross *et al.*, 2005].

[10] The ATOFMS, as further discussed in subsequent sections, is a qualitative instrument. The peak heights in the bipolar mass spectra are related to the abundance of ions generated in the desorption and ionization beam. They can be affected by the distribution of components through the aerosol (i.e., surface or interior), the ionization efficiency of that specific material, and other properties of the particle matrix [Gross *et al.*, 2000; Wenzel *et al.*, 2003; Murphy, 2007]. Without extensive laboratory determination of these effects mass spectra cannot be directly related to the component quantities [Cziczo *et al.*, 2001; Dessiaterik *et al.*, 2003].

[11] Although sizing information of every detected particle is available it is noted that this size is not directly related to the DMA2 size. Humidified particles leaving DMA2 can experience a warming or cooling from the temperature of the DMA housing to room temperature in the capillary tubing, leading to condensation or evaporation. Evaporation can also take place in the aerodynamic lens inlet due to lower than ambient pressure [Zelenyuk *et al.*, 2006].

[12] Approximately 260 nm particles were found to be the smallest size with a combined high aerodynamic transmission efficiency, light scattering intensity, and hit rate. In addition, this size is within the range where it can be assumed that the particle is largely desorbed during the desorption/ionization process [Weiss *et al.*, 1997]. For this reason 260 nm particles have been selected as the incoming dry aerosol size (i.e., D_0). This condition was also a maximum limit due to arcing in the 2nd DMA at the highest

voltages required for the largest growth factors (i.e., the highest humidities).

[13] It is noted that in a typical ambient aerosol distribution 260-nm particles generally belong to a portion of the distribution above the number maximum and often closer to the mode of the volume distribution [Weingartner *et al.*, 1999]. This size range is regarded as representative of accumulation mode particles.

[14] During the experiments in the laboratory and in Zurich DMA2 was operated in a scanning mode. Scans were performed in the range from 0.8 to 1.8 D_0 over a period of 6 minutes. At the JFJ, due to low particle concentrations, DMA2 was stepped with an increment of delta GF = 0.1 covering the GF range in 6 minutes. Additionally, a 6-minute full-range scan was done approximately once per hour to obtain the overall GF distribution. Before all measurements operation of the HTDMA system was verified with pure ammonium sulfate particles.

2.2. Proof of Concept Experiments

[15] Before field deployment the new setup was tested in the laboratory under controlled conditions. An externally mixed dual-component aerosol with different hygroscopic properties was generated with two custom-built atomizers run in parallel. One atomizer contained 260 nm PSL spheres (Duke Scientific) in distilled water. The other atomizer contained an aqueous NaNO_3 solution (Sigma-Aldrich, >99% pure). The generated aerosol was sampled with the connected setup where DMA1 selected for an input diameter of 260 nm. DMA2 was used in scanning mode and a size distribution was derived from the CPC counts. A bimodal size distribution with distinct peaks for both the PSL and the NaNO_3 particles was observed. The ATOFMS sampled in parallel to the CPC and showed a time (i.e., growth factor) dependent sequence for the composition. In Figure 2 a typical HTDMA scan is shown with the corresponding ATOFMS spectra. In a second test experiment the setup was used with aerosols having intermediate hygroscopic properties. This was done by filling a single atomizer with a solution containing NaNO_3 and 260 nm PSL spheres. The HTDMA was used in a scanning mode and DMA1 diameters of 260, 280 or 300 nm were selected. Thus particles passing DMA1 consisted of either pure

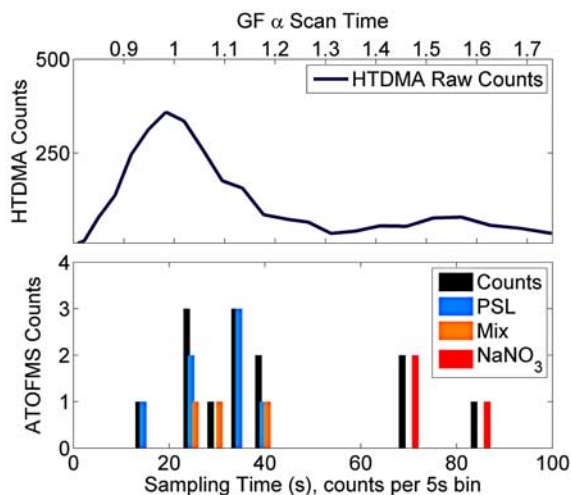


Figure 2. An example of a HTDMA scan and related ATOFMS mass spectra. (a) HTDMA scan of externally mixed 260 nm NaNO_3 and PSL particles. The entire GF range was scanned within a specific time interval; the sampling time of the ATOFMS is referenced to the scan time by a shift to account for transmission time. (b) Detected ATOFMS counts within this time interval (black) and their composition (blue, PSL; red, NaNO_3 ; orange, mixed PSL with NaNO_3). Mixed particles are due to sodium found in the PSLs and as a contaminate of the aerosol production process [Dessiatierik *et al.*, 2003].

NaNO_3 or were coated PSL spheres with 0, 10, or 20 nm NaNO_3 radial thickness. HTDMA scans for the three different DMA1 diameters are shown in Figure 3, panel A. While the GF at 82% RH for the pure NaNO_3 mode remained stable at 1.6, the GF of the less hygroscopic mode (more or less coated PSLs) changed with the coating thickness. It should be noted that, even in the case of nominally uncoated PSLs, some residual hygroscopic material is

expected to coat the surface due to the production process and the nonideal separation by a DMA (i.e., there is a finite width to the DMA transfer function). For this reason there is a GF slightly larger than unity associated even with nominally uncoated PSLs. These results are consistent with the experiments of Buzorius *et al.* [2002] and follow the theoretical hygroscopicity behavior of these internally and externally mixed particle types.

[16] As previously mentioned, ATOFMS mass spectra provide qualitative information about single particle chemical composition. An understanding of relative quantity can, however, be gained by comparing peak ratios to the overall mass spectral area. This has been shown by Middlebrook *et al.* [2003] and Murphy *et al.* [2006], who compared data from single particle mass spectrometers with quantitative instruments such as particle-into-liquid samplers (PILS). For this study this ability can be seen in the analysis of ATOFMS mass spectra from the lower growth mode (i.e., PSLs with variable coating). Roughly 100 mass spectra were collected for each coating thickness and the spectra have been averaged and normalized to a relative area of 1. In Figure 3b, a portion of the positive mass spectra is shown for each selected DMA1 diameter. The Na^+ peak at $m/z = 23$ (NaNO_3 fragment) is highest with thickest NaNO_3 coating. Note that, as shown in Middlebrook *et al.* [2003] and Murphy *et al.* [2006], the relative quantity need not follow a linear relationship (i.e., twice the abundance of material need not result in a doubling of the signal). This is true of this simple system as well as the more complex mixtures observed in the atmosphere. Conversely, the relative intensity of peaks associated with PSLs, such as $m/z = 27$ (C_2H_3) or $m/z = 36, 37, 38, 39$ ($\text{C}_3, \text{C}_3\text{H}, \text{C}_3\text{H}_2, \text{C}_3\text{H}_3$), decreases.

2.3. Sampling Sites

[17] After the proof of concept experiments the setup was deployed for two field studies. A first data set was obtained in the urban Zurich area. Samples were taken from an isokinetic inlet located at the ETH laboratory which is at

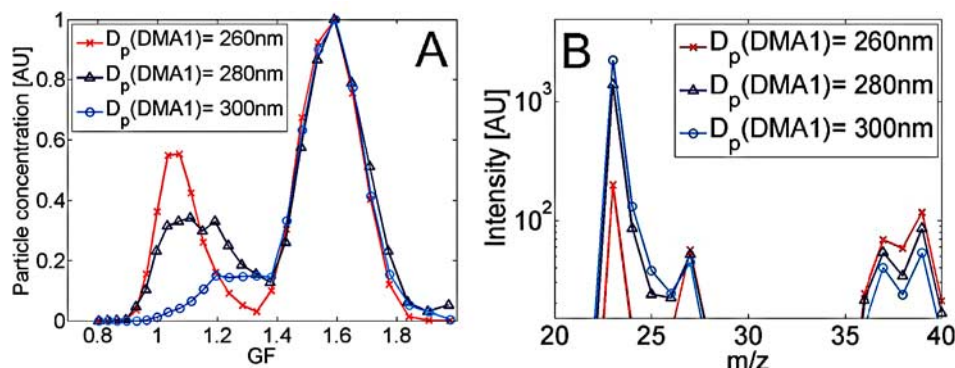


Figure 3. (a) HTDMA counts of atomized internally and externally mixed PSL and NaNO_3 particles as a function of growth factor for different DMA1 diameters. DMA1 diameter is thus related to the NaNO_3 coating of the PSL particles which are all of 260 nm diameter (i.e., particles with GF 1.6 are pure sodium nitrate, whereas the smaller GF is attributed to PSLs with variable coatings from 0 to 20 nm radial thickness). (b) ATOFMS positive polarity mass spectra showing the Na^+ peak ($m/z = 23$) intensity for different DMA1 diameters which changes with the NaNO_3 coating thickness. The positive 36–38 mass peaks are due to the PSL material and are anticorrelated with the coating thickness.

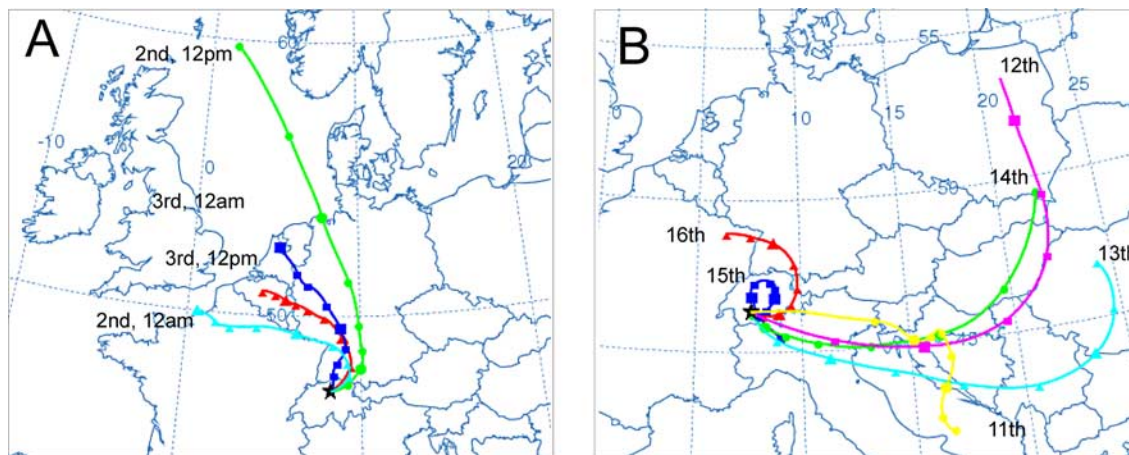


Figure 4. (a) 48 h back trajectories for Zurich from 2 to 3 February 2007 initialized in 12-h intervals. Date indicates the day when trajectories reached Zurich. (b) 48 h back trajectories for the JFJ from 11 to 17 March 2007 initialized in 24-h intervals. Date indicates the day when trajectories reached the JFJ. All trajectories are generated with the HYSPLIT model. Small symbols represent 6 hourly intervals in the back trajectory.

485 m above sea level (msl) and close to the city center. Data was taken from 1 to 3 February 2007. A total of ~ 3500 single particle mass spectra were obtained. During the measurement period an inversion layer was present. Because of this, much of the aerosol loading was of local origin. Regional influence for the sampling period was determined with the National Oceanic and Atmospheric Administration (NOAA) HYSPLIT model [Draxler and Rolph, 2003] and this is shown in Figure 4. The back trajectories suggest that the air mass originated in a region to the north–west. HTDMA scans during the measuring period showed that two particle growth modes were predominate, the first centered at GF 1.0 and a second, larger, one at GF 1.4.

[18] The second ambient study was performed at the remote high alpine research station JFJ located at 3580 msl in the Swiss Alps. The deployment of this setup was part of the 6th Cloud and Aerosol Characterization Experiment (CLACE 6). Due to its remote location and altitude the JFJ is rarely affected by local particle emission and, during wintertime, it is often situated in the free troposphere [Baltensperger *et al.*, 1997; Collaud Coen *et al.*, 2007]. These properties make it a counterexample to urban Zurich. Measurements were taken from 9 to 17 March 2007. The annual aerosol concentrations at the JFJ are lowest during wintertime [Weingartner *et al.*, 1999]. During the measured period the prevailing air masses had particle concentrations ranging from less than 100 to ~ 600 cm^{-3} . Due to these extreme conditions only 54 particles were chemically analyzed with the ATOFMS. Almost all of these particles were detected between 11 and 16 March 2007. The air mass history for this interval is shown in Figure 4. During the measurement period air masses originated from central and eastern Europe. As has been shown previously by Sjogren *et al.* [2007] the GF distribution at the JFJ during wintertime, including particles with $D_0 = 250$ nm, is generally bimodal with one mode at GF 1.4–1.5 and a smaller second mode at

GF 1.0–1.1. This bimodal behavior was also found for $D_0 = 260$ nm particles during this study.

3. Results and Discussion

3.1. Zurich

[19] The Zurich data set consists of 3534 bipolar high signal to noise mass spectra of individual aerosol particles. About 90% of the measured particles were centered around a GF of ~ 1.4 whereas the remaining 10% were centered around a GF of ~ 1.0 . A few particles with GFs lower than 1.0 were detected. It is assumed that these particles belong to the tail of the particle distribution at 1.0 as it is known that fractal particles, e.g., fresh soot, can collapse during the humidification process [Mikhailov *et al.*, 2006; Weingartner *et al.*, 1997].

[20] Evaluation of the mass spectra showed that most particles, regardless of GF, were internally mixed. A detailed examination of the mass spectra was performed by binning according to the particle GF in steps of 0.05 and then determining whether specific compounds were present. Ubiquitous compounds found in the negative mass spectra were sulfates and nitrates as well as peaks associated with elemental carbon (EC) and organics [Murphy and Thomson, 1997a]. Besides sulfate (e.g., HSO_4^-), nitrate (NO_2^- and NO_3^-) and EC peaks (C_n , where n is an integer), organic fragment peaks -26 (C_2H_2^- or CN^-) and -42 ($\text{C}_2\text{H}_2\text{O}^-$ or CNO^-) were analyzed. The cluster peak -125 (likely $\text{NO}_3\text{HNO}_3^-$ and a marker for nitrates), which was often found in the mass spectra, was also analyzed. The predominant compounds found in positive mass spectra were potassium, metals, and EC peaks [Murphy and Thomson, 1997b]. The potassium signal was likely due to biomass burning from wintertime domestic heating which is common in Switzerland [Lanz *et al.*, 2008]. In these analyses mineral dust and fly ash (i.e., particles which exhibited refractory material peaks such as aluminum, calcium, silicon, iron, etc.) and biomass (spectra containing potassium,

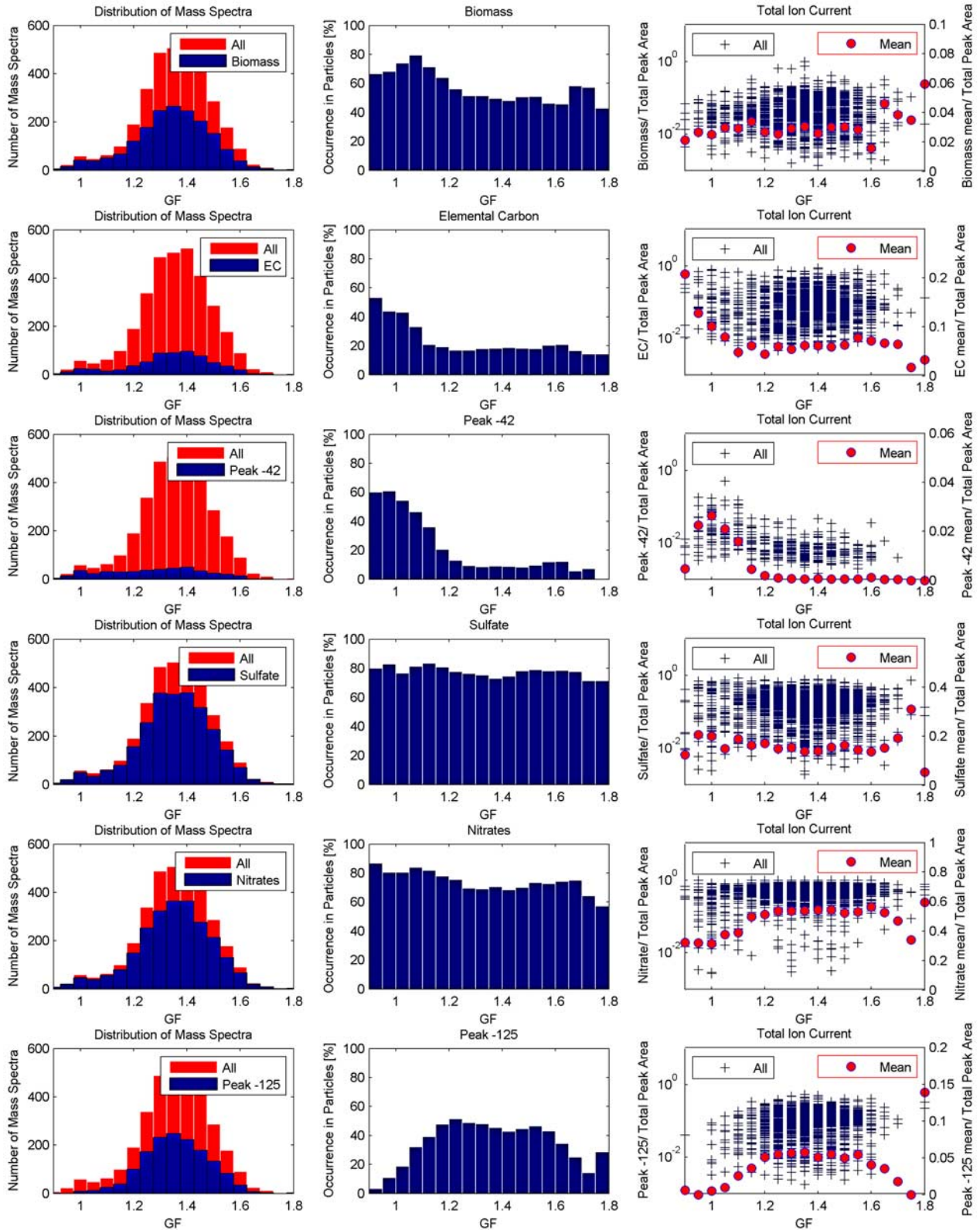


Figure 5

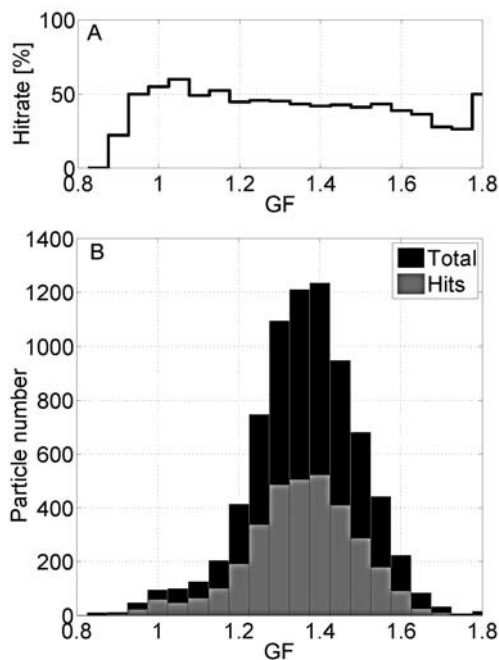


Figure 6. (a) Particle hit rate, defined as the percentage of particles which generated a mass spectrum versus total particles detected, as a function of GF. (b) The total number of particles sized with the ATOFMS during the sampling period and the subset which generated a mass spectrum. Although fewer particles are present with low GF these generated a mass spectrum at a rate only a few percent higher than those with higher GF.

organic, and EC fragments) are identified from the positive spectra. It is important to note that the appearance of EC peaks in a mass spectrum does not define that the particle is made of pure EC. EC peaks can be derived from biomass burning and diesel soot or by “charring” of organic material in the desorption laser. Both peaks -26 and -42 have been previously observed in ATOFMS mass spectra, e.g. *Holecak et al.* [2007] who detected them in rainwater samples. The authors assumed the peaks to be CN^-/CNO^- (i.e., organic nitrogen species).

[21] Figure 5 shows the occurrence of six of these chemical compounds (from top to bottom: biomass, EC, peak -42 , sulfates, nitrates and peak -125) as a function of GF. A minimum peak height with a 3:1 signal-to-noise ratio determined the presence or absence of a compound peak. One feature that can be seen from the figure is that biomass, EC, and peak -42 are enriched in the low GF range. Additional data analysis for peak -26 (CN^- or C_2H_2^-), which is not shown here, indicated the same trend. For

sulfates and nitrates limited GF dependence was observed. Sulfate was a constituent in about 80% and nitrate was present in about 70–80% of all particles. The slight enhancement of nitrates in the low GF mode can be at least partly attributed to the high affinity of nitrates for mineral dust [*Laskin et al.*, 2005] which is enhanced in these particles as described in the next section.

[22] One uncertainty introduced in these results is the possible bias in detection efficiency of particles with different components. As previously mentioned, mass spectra are dependent on the complex mixture of compounds found within a particle. Mass spectral production (i.e., the production of ions above the background noise) can thus be affected by the particle matrix [*Cziczo et al.*, 2001]. Water evaporation and/or condensation within aerodynamic lenses has been shown to affect mass spectrometer signal [*Zelenyuk et al.*, 2006] but there are no known chemical biases related to transmission. The concern is that these data could be biased if particles in a certain mode had a composition which significantly enhanced or reduced the production of mass spectra. In Figure 6 the particle hit rate, defined as the ratio of particles which produced a mass spectrum versus total detected particles, is presented as a function of GF. Panel B shows the total number of particles sized with the ATOFMS during the sampling period and the subset which produced a mass spectrum. Particles with a GF of ~ 1 generated spectra $\sim 55\%$ of the time whereas those particles with a GF of ~ 1.4 did so with a rate of $\sim 45\%$. This difference can most probably be attributed to the higher frequency of easily ionizable refractory material in the low GF particles (e.g., mineral dusts and soot). The hit rate difference also shows that any relative overvaluing of the low GF mode is less than 20%.

[23] These results can be compared with previous studies although methodology differences exist. One difference is that previous studies did not include direct measurements of aerosol composition as a function of hygroscopic growth [*Baltensperger et al.*, 2002; *Dusek et al.*, 2006]. *Baltensperger et al.* [2002] reported a mean fraction of 33% in the less hygroscopic mode, however this related to 100-nm particles. Here results are presented for 260-nm particles. In Zurich, the size distribution of fresh soot particles from traffic shows a mode around 80 nm [*Imhof et al.*, 2005]. Thus particles with a diameter of 260 nm have grown considerably by condensation, which explains the high fraction of sulfate and nitrate containing particles. In addition, the Zurich winter aerosol contains a high fraction of soot particles from wood combustion [*Lanz et al.*, 2008]. These particles include substantial amounts of water soluble organic carbon, contributing to an enhanced growth factor of the freshly emitted particles.

Figure 5. Aerosol chemical composition as a function of growth factor found in Zurich. From top to bottom row analyses for six chemical compounds are presented. First column shows the GF distribution of all 3534 mass spectra and the relative occurrence of the analyzed compound. Second column presents the occurrence of each compound normalized to the number of spectra as a function of GF (e.g., EC is observed to be present in 50% of the low growth factor particles but less than 20% of those in the high growth factor). Third column shows the compound peak to total peak height ratio for each single mass spectra as a function of GF (left scale) and the average peak height ratio for each GF bin (right scale; e.g., EC is not only found in a higher percentage of low GF particles but is also a larger percentage of the ions in the mass spectrum). See text for further details.

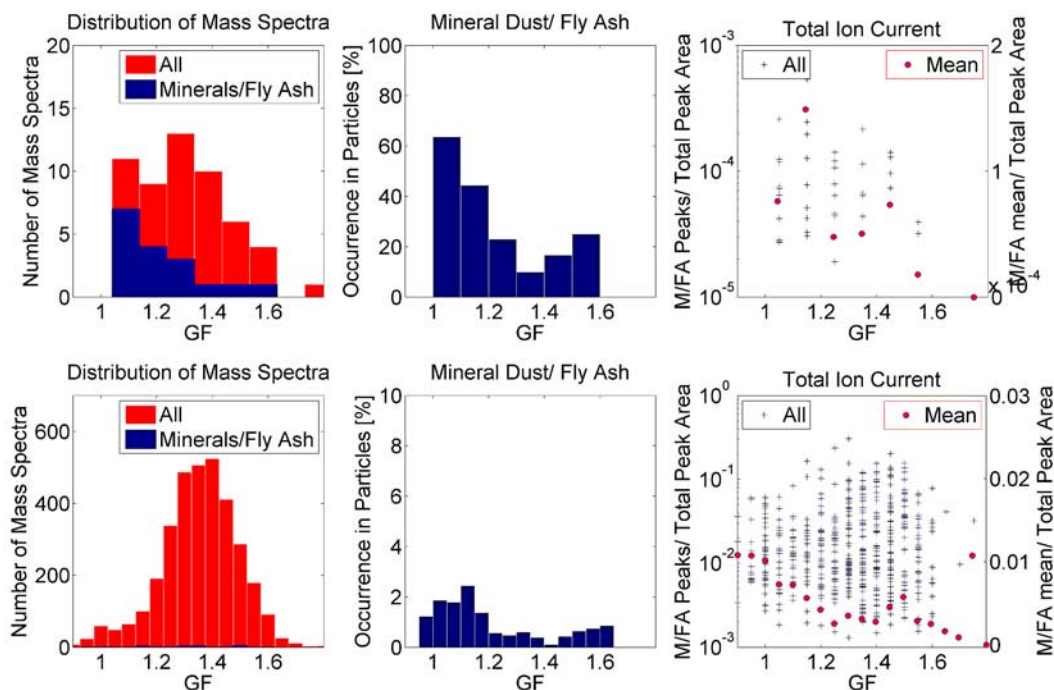


Figure 7. Occurrence of mineral dust and fly ash (MD), a function of growth factor where the three columns are analogous to those found in Figure 5. Bottom row shows Zurich data; the left panel shows the GF distribution of all 3534 mass spectra and the subset of particles with features related to MD. The middle panel presents the occurrence of MD normalized to the number of spectra as a function of GF. Third column shows the ratio of MD peaks to total peaks for each single mass spectra as a function of GF (left scale) and the average peak height ratio for each GF bin (right scale). Top row shows the results for the JFJ. Note that the majority of MD particles are found in the low hygroscopicity mode.

[24] Regardless, the occurrence of sulfate and nitrate in the less hygroscopic mode is counterintuitive as both compounds are commonly assumed to be only associated with more hygroscopic aerosols. To investigate if the quantity of these compounds was higher for hygroscopic aerosols an analysis of the peak heights was performed for all compounds. In the third column of Figure 5 the peak ratios of the compound to the total peak area is presented for all spectra as a function of GF. Spectra without the compound are also included in this average (i.e., those with a zero value) which leads to low average values for some compounds in certain bins. The highest peak ratios for biomass, EC, and peak -42 are found in the low GF range. Thus these compounds are found to be more frequently in the low GF mode aerosols and their relative abundance is also higher. The peak -42 data in particular show a higher percentage in the low GF range with peak ratios an order of magnitude larger than for the high GF. The same trend applies for the peak -26 data (not shown). Two caveats should be mentioned. First, the number of low GF particles is lower, by almost an order of magnitude, than the high GF mode. Second, it is possible that the deliquescence point of some aerosols may have been slightly higher than the 82% RH used in the HTDMA [Seinfeld and Pandis, 2006]. This is unlikely, however, due to the large degree of internal mixing of inorganic and organic compounds as has been shown for mixtures of water soluble compounds in laboratory experiments [Marcolli et al., 2004; Marcolli and Krieger, 2006].

[25] For the sulfate analysis the masses of the most common peaks were summed ($m/z = -80(\text{SO}_3^-)$, $-81(\text{HSO}_3^-)$, $-97(\text{HSO}_4^-)$, $-99(\text{HSO}_4^-)$, $-111(\text{CH}_3\text{SO}_4^-)$, $-177(\text{HSO}_4^-\text{SO}_3^-)$, and $-195(\text{HSO}_4\text{H}_2\text{SO}_4^-)$ [Murphy and Thomson, 1997a]). A comparison of all sulfate peaks versus only peak -97 and -80 showed that the latter had the highest abundance ($>80\%$). From the peak ratios it can be seen that sulfate is a major compound in the spectra. On average $\sim 20\%$ of the mass spectral peak area was sulfate. For nitrates the highest peak ratios were found in the more hygroscopic growth mode with an average area of $\sim 50\%$. It can be seen from Figure 5 that the peak ratio distribution for sulfate as well as for nitrates was relatively stable with few outliers. The highest peak ratios for $\text{NO}_3\text{HNO}_3^-$ are found in the GF range of 1.2 and higher. It has been previously observed that, depending on the air mass, particles may contain the cluster peak $\text{NO}_3\text{HNO}_3^-$ or only the nitrate fragments [Murphy and Thomson, 1997a].

[26] Mineral dust and fly ash were also observed. An analysis is shown in Figure 7. Only a small percentage of the aerosols contained such refractory material ($\sim 2\%$) but these were enhanced in the particles with a low GF. The observation that EC and biomass are enhanced in less hygroscopic particles is consistent with previous studies [Baltensperger et al., 2002]. Fresh diesel soot particles are known to be nonhygroscopic [Weingartner et al., 1997]. With aging processes (e.g., condensation and agglomeration) these particles are known to acquire soluble compounds and become more hygroscopic [Petters et al., 2006].

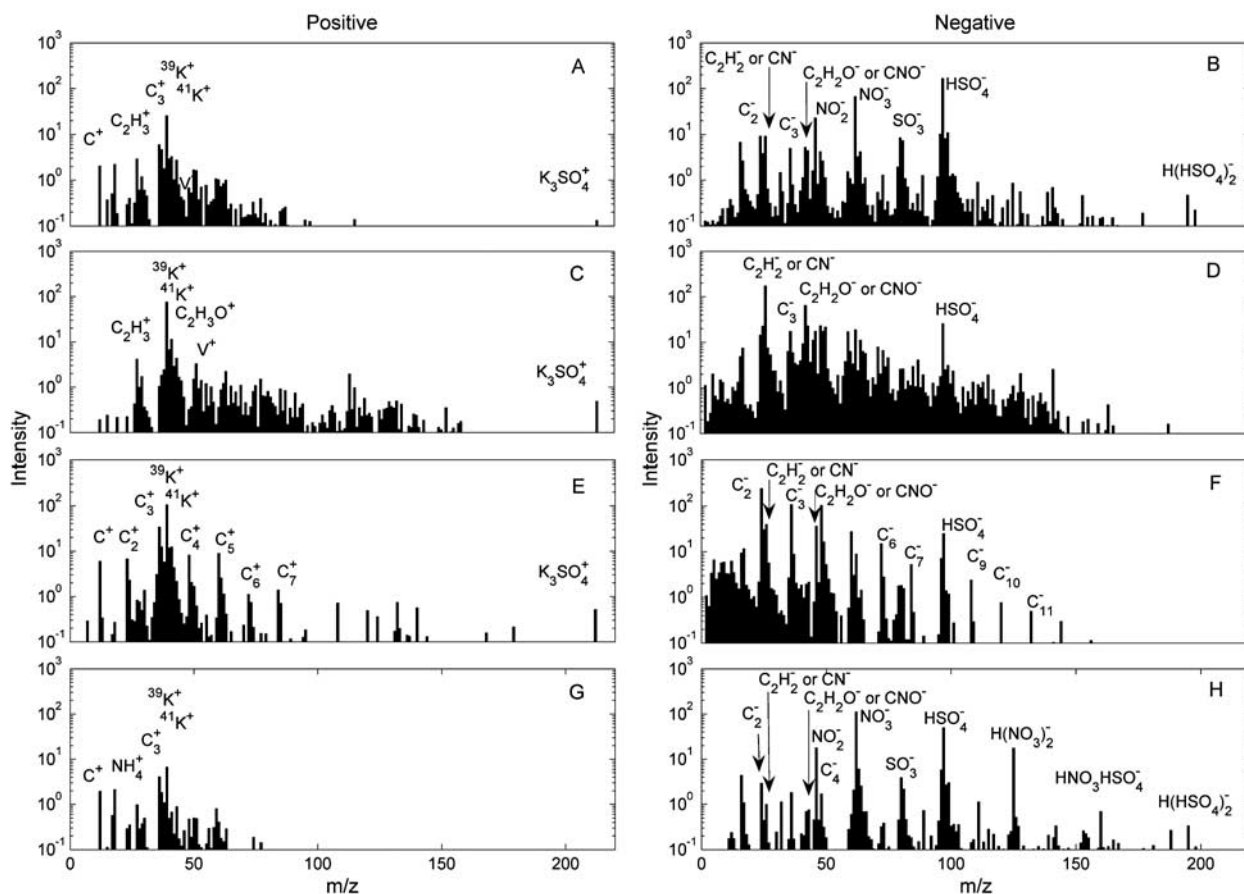


Figure 8. Mass spectra of aerosol particle clusters. (left) Positive mass spectra. (right) Negative mass spectra. (a–f) Cluster centers for Zurich particles with GF 1.0. Most particles were internally mixed sulfate, nitrate, EC, and potassium (a). Some were dominated by organics (b) and some contained mainly EC (c). (g and h) Cluster center for Zurich particles with GF 1.4. Most particles contained few EC peaks, but potassium and several sulfate and nitrate cluster peaks.

This is supported in the results presented here for the particles with a GF of ~ 1.4 . These particles contain sulfates and nitrates and are often internally mixed with EC and/or biomass residue.

[27] A second analysis step was performed by separating the particles in the range GF 0.9 to 1.1 (particle group GF 1) and GF 1.3 to 1.5 (particle group GF 1.4). Specifically, these groups were categorized using the cluster analysis open source software Enchilada [Gross *et al.*, 2006]. The group GF 1 contained 167 particles and these were clustered into 10 categories. Approximately 80% of all particles could be further combined into three main groups. The cluster centers of the three groups are presented in Figure 8. Group 1, found in panels A and B, consisted of internally mixed particles containing sulfates, nitrates, EC, the biomass indicator potassium, some refractory compounds, and organic fragments. The peak height proportions varied from spectra to spectra. The total number of group 1 particles was 108 (i.e., 65% of the low GF aerosols). Group 2, panels C and D, was dominated by organics and hydrocarbons with lesser potassium, nitrate and sulfate contribution. Group 2 represented 6% of the low GF mode. The cluster center of group 3, panels E and F, showed a typical combustion generated particle consisting of EC and often potassium.

Sulfates and nitrates were often present as well. Group 3 also represented 6% of the low GF mode. A temporal plot of the three showed that group 1 particles were detected throughout the sampling period whereas the particles from group 2 were mainly detected during nighttime. Particles from group 3 were found mainly during the evening of 2 February (Friday); these may be related to vehicle emissions at “rush hour.” The fourth largest category (not shown), 3% of the total, can be loosely defined as mineral dust and fly ash due to the presence of metallic ions. The diversity of elements and peak heights makes a clear cluster center for the remaining particles impossible.

[28] A total of ~ 1850 particles can be attributed to the GF 1.4 bin. All of these particles were internal mixtures of sulfate, nitrates, potassium and organics. The peaks varied among the particles in a continuous manner such that any could be the largest or smallest. Due to this variety subclustering did not simplify the data. Composition differences with time during the sampling period were not observed. Figure 8 panels G and H show the cluster center for $>98\%$ of the GF 1.4 particles. One striking feature is that the only obvious visible difference between the group 1 particles in the GF 1 mode and the GF 1.4 particles is an enhancement in the organic peaks (e.g., -26 (C_2H_2 or

CN) and -42 (C_2H_2O or CNO)) when compared to the EC (-24 (C_2) and -36 (C_3)) peak heights.

3.2. JFJ

[29] The 54 single particle mass spectra obtained at the JFJ were analyzed in the same manner as the Zurich data. The small number of spectra renders these as statistically insignificant; instead, they are shown here to contrast what was observed in the urban Zurich environment. Due to the small number the particles were sorted in GF bins in steps of 0.1. In Figure 9 the analyses for biomass, EC, peak -42 , sulfates, nitrates, and peak -125 are presented. Biomass burning related compounds were present in about 50% of the detected particles and were more often found in particles with a GF in the range of 1.4 than for particles with GF 1. This may be explained by aged biomass burning particles (i.e., those that acquired soluble material). The peak ratios were similar for all GF bins. EC peaks were present in many particles and the peak ratios also did not show a significant trend. The results for peak -42 (organic fragment) showed the same clear trend as in the Zurich data; this peak was found in 100% of hydrophobic particles but only 50% of the hydrophilic. Additional analysis of peak -26 , which is not presented here, showed the same trend. Sulfate was found in almost all particles, in agreement with the Zurich results. Sulfates were the dominant compounds, accounting for up to 50% of the peak area.

[30] Both the sulfate and nitrate behavior was, again, contrary to common assumptions. The sulfate peak ratios did not show any significant trend, as was the case for Zurich. Nitrates were only found in about 40% of all particles, predominantly in the less hygroscopic mode. The highest nitrate peak ratios were found in the low GF mode range but, in comparison to Zurich, only a few percent of the peak area was made up by nitrates. The nitrate occurrence in the low GF mode can again be partially explained by the observation that at this high altitude site nitrate is associated with mineral dust often due to neutralization of nitric acid at the basic particle surface. The cluster peak $NO_3HNO_3^-$ was found in only about 25% of in the JFJ particles, and the peak ratios of this compound were generally small. The distribution did not follow the trend observed for Zurich data where $NO_3HNO_3^-$ was enhanced in hydrophilic particles. This is in agreement with the fact that the nitrate to sulfate ratio is much lower in the free troposphere than in the planetary boundary layer, resulting in very low concentrations of ammonium nitrate [Henning *et al.*, 2003].

[31] The occurrence of mineral dust and fly ash in JFJ particles is shown in Figure 7; 60% of particles with GF 1 contained components associated with mineral dust or fly ash. At the higher GFs the fraction of particles containing mineral dust and fly ash was much smaller. The results for refractory material agree well with former observations. For example, Sjogren *et al.* [2007] showed that during Saharan dust events (SDE) a low GF mode was seen in HTDMA data (for $D_0 = 250$ nm) at the JFJ. We can exclude a major SDE for the sampling period based on the back trajectories (see Figure 4b). The result here is that background atmospheric mineral dust largely exhibits the same nonhygroscopic behavior. The same was true of the urban Zurich data set: although minerals were rarely found in the urban air

when they were they were enhanced in particles from the nonhygroscopic GF mode.

[32] Due to the small amount of data it was not possible to do a cluster analysis of the JFJ mass spectra and diurnal variations could not be monitored. Visually, most of the particles from the nonhygroscopic mode were similar to the group 2 Zurich particles. Particles in the GF 1.3 to 1.5 range were internally mixed in various combinations. Potassium and sulfate species were dominant. Nitrates and organics were less common, which is different from the Zurich data set.

4. Atmospheric Implications

[33] We have designed, built, and tested an apparatus to determine the chemical composition of atmospheric particles as a function of hygroscopic growth both in situ and in real time. Subsequently, we deployed this setup in two contrasting locations in Switzerland during the same winter-time: the urban Zurich environment and the free tropospheric JFJ high alpine research station. The field results show that in urban Zurich air most particles contained sulfates and nitrates independent of their GF. Sulfates were also ubiquitous at the JFJ. It was also found that certain peaks, namely organic fragments -42 and -26 , were predominantly found in less hygroscopic particles. EC, biomass, and mineral dust signatures were also found to be enhanced in less hygroscopic particles.

[34] The relationship between aerosol chemical composition and hygroscopic growth is an important factor in several atmospheric processes. The hygroscopic behavior of simple species like salts and certain organics in different mixing states is well known [Kreidenweis *et al.*, 2005; Koehler *et al.*, 2005; Svenningsson *et al.*, 2006; Topping *et al.*, 2005]. The hygroscopicity of particles with more complex high molecular weight organic molecules, such as humic-like substances (HULIS), has been recently investigated in the laboratory [Chan and Chan, 2003; Gysel *et al.*, 2004; Dinar *et al.*, 2007]. The current work should be considered an extension of these studies to the field. Specifically, this technique can be used to probe the hygroscopicity of vastly more chemically complex atmospheric aerosols that have aged and/or participated in heterogeneous chemical reactions. This work can help to focus our efforts in future laboratory studies. As such, this technique has been shown to be an important tool for ongoing investigations of aerosol radiative effects, heterogeneous chemistry, and cloud activation.

[35] The most surprising result of these studies is the frequent occurrence of species normally considered soluble (e.g., sulfates and nitrates) in low GF particles. Our results agree with previous work, such as that of Baltensperger *et al.* [2002], who suggested that nonhygroscopic particles (i.e., $GF \sim 1$) were fresh emission materials, for example elemental carbon. Sjogren *et al.* [2007] noted that mineral dusts can also be nonhygroscopic and this is, likewise, supported by these data. This work diverges from that of Baltensperger *et al.* [2002] who concluded that once gas phase uptake of soluble species, such as sulfate, occurred or coagulation took place, a particle would increase its hygroscopicity. In both the Zurich environment and at the JFJ sulfate was present on most particles, regardless of GF.

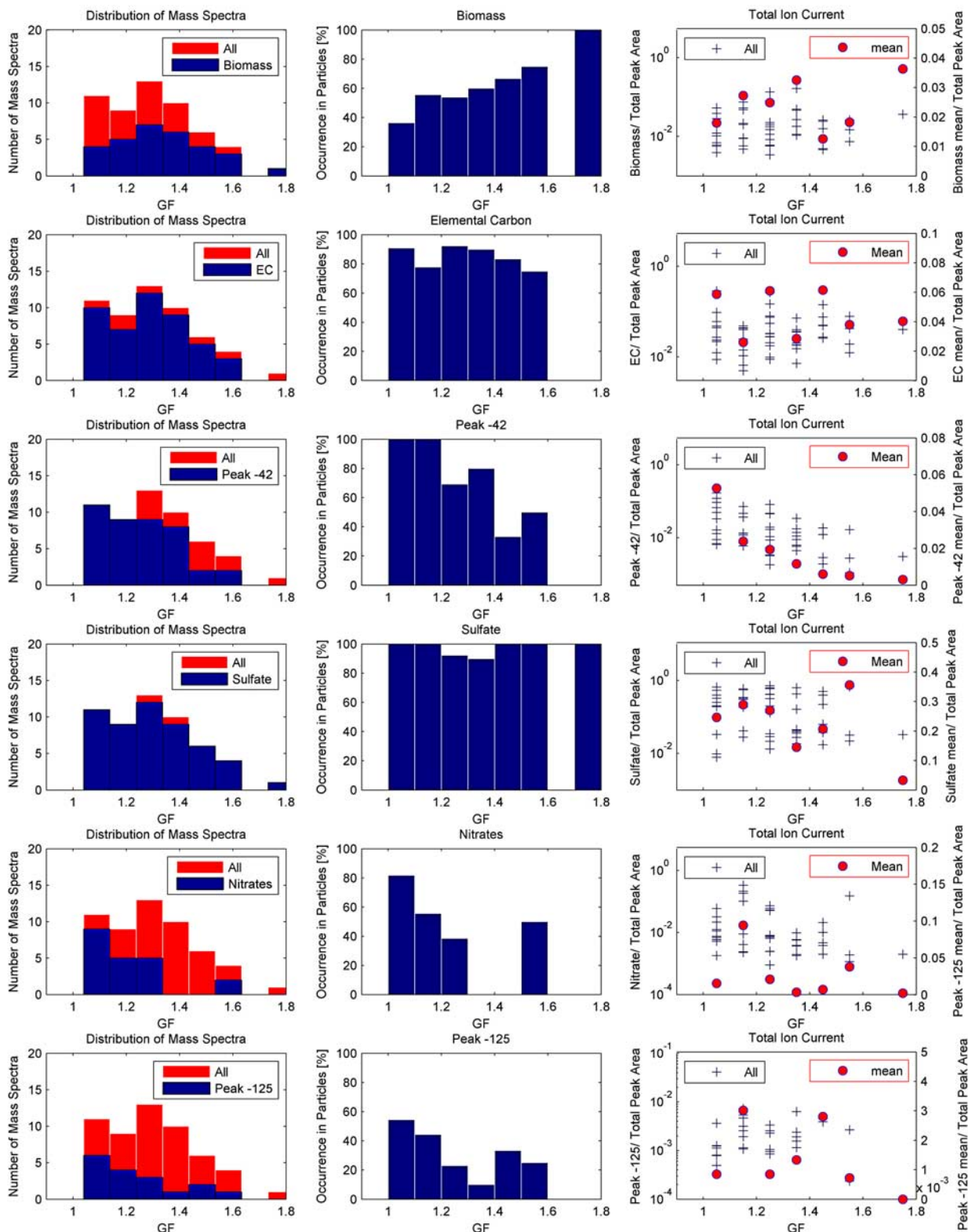


Figure 9. Aerosol chemical composition as a function of growth factor found at the JFJ, analogous to what is shown for Zurich in Figure 5. From top to bottom row analyses for six chemical compounds are presented. First column shows the GF distribution of all 54 mass spectra and the relative occurrence of the analyzed compound. Second column presents the occurrence of each compound normalized to the number of spectra as a function of GF. Third column shows the compound peak to total peak height ratio for each mass spectra as a function of GF (left scale) and the average peak height ratio for each GF bin (right scale). See text for further details.

Although single particle mass spectrometry is predominantly a qualitative technique, the sulfate peak ratio did not change with GF, implying that the relative abundance of sulfate did not significantly change. Particle hit rate remained largely constant across the GF modes so the aerosol matrix cannot fully explain these results, either.

[36] There are several possible explanations for the surprising finding of sulfate and nitrate in the low GF mode. First, it is possible that the soluble material was “trapped” by a low-hygroscopicity coating, such as from organic material. This would also explain the relative increase in organic fragments with low growth factor. It has been previously observed in electron microscopy studies that sulfate salt crystals can be found encapsulated in organic material [Johnson *et al.*, 2005]. On the other hand, Hansson *et al.* [1990] were not able to suppress hygroscopic growth of NaCl particles by coating with hydrophobic organics. Chan and Chan [2007] recently showed that water-insoluble organic coatings on $(\text{NH}_4)_2\text{SO}_4$ particles can have an effect on the water uptake, although that was only the case for small residence times at high RH conditions. A second theory is that the sulfate may be bound in a low-solubility form, for example in an organo-sulfate material. Third, it cannot be excluded that the mass fraction of sulfate was small on almost all particles throughout both measurement periods. For example, a particle with only 10% sulfate and 90% insoluble material has a growth factor of <1.1 at $\sim 83\%$ RH. Such a particle would show up in the lowest GF bins presented here even without any films. Should this have been the case it remains unclear why there was little difference in sulfate signal across the GF range studied here.

[37] These results suggest that the common assumption that the simple presence or absence of certain compounds determines particle hygroscopicity should be reevaluated. The simple presence or absence of hygroscopic material does not appear to dictate hygroscopicity. As such the uptake of soluble species by hydrophobic particles cannot be assumed to immediately lead to more hygroscopic behavior. Models which make the assumption of an increase in particle hygroscopicity with atmospheric aging for initially hydrophobic aerosol particles may not completely capture the behavior of atmospheric aerosols. Ultimately, laboratory measurements should be undertaken to determine if organic coatings or organo-sulfate materials can explain these results or if another process is responsible.

[38] The results for nitrates have similarities and differences to those for sulfates. While nitrates do show an increase of peak area with increasing GF they were also observed in nonhygroscopic particles. At the JFJ they were enhanced in the GF = 1 particles and this was likely due to the fact that mineral dust particles preferentially took up gas-phase nitric acid, as has been observed in field [Henning *et al.*, 2003] and laboratory studies [Laskin *et al.*, 2005]. It should also be noted that matrix effects and ionization efficiency may mean that a larger quantity of nitrate than sulfate may have existed on the sampled particles. To explore this further and determine if these findings are universal field studies in more varied regions, for example those dominated by mineral dusts, are needed. The nature of the nitrate material observed in the low GF mode is also of interest. Nitrate salts are known to be hygroscopic so the form of the material observed here is of interest. Future

work should also be directed at expanding the size and humidity range over which these measurements can be performed.

[39] Both at the JFJ and in Zurich refractory material such as mineral dust was enhanced in nonhygroscopic particles. From previous studies it is known that mineral dust is a major compound found in ice nuclei (IN; e.g., DeMott *et al.* [2003]). An improved understanding of ice cloud formation is also an important factor for reducing the uncertainty associated with the indirect effect [Forster *et al.*, 2007]. Several heterogeneous ice nucleation modes have been identified in the atmosphere, some of which act only on bare refractory surfaces (deposition) while other act from within droplets (immersion). Our finding that mineral dust is most often found in the nonhygroscopic mode implies that these particles are more likely to act as deposition or contact IN. Also of atmospheric interest, this implies that a property that makes for a good IN (low hygroscopicity) simultaneously makes for a bad CCN. Put another way, effective liquid water cloud nuclei and good ice nuclei appear to be largely mutually exclusive.

[40] **Acknowledgments.** This work was supported by ETH internal research funding, PNNL Aerosol Initiative, and European Commission project EUSAAR (European Supersites for Atmospheric Aerosol Research). We gratefully thank Markus Gälli for ATOFMS technical support and Deborah Gross, Fred Brechtel, Alex Laskin, and Alla Zelenyuk for useful discussions. We also appreciate the support of all CLACE participants and the International Foundation High Altitude Research Stations Jungfraujoch and Gornergrat (HFSJG).

References

- Baltensperger, U., H. W. Gäggeler, D. T. Jost, M. Lugauer, M. Schwikowski, E. Weingartner, and P. Seibert (1997), Aerosol climatology at the high-alpine site Jungfraujoch, Switzerland, *J. Geophys. Res.*, *102*, 19,707–19,715.
- Baltensperger, U., et al. (2002), Urban and rural aerosol characterization of summer smog events during the PIPAP0 field campaign in Milan, Italy, *J. Geophys. Res.*, *107*(D22), 8193, doi:10.1029/2001JD001292.
- Brechtel, F. J., and S. M. Kreidenweis (2000a), Predicting particle critical supersaturation from hygroscopic growth measurements in the humidified TDMA: Part I. Theory and sensitivity studies, *J. Atmos. Sci.*, *57*, 1854–1871.
- Brechtel, F. J., and S. M. Kreidenweis (2000b), Predicting particle critical supersaturation from hygroscopic growth measurements in the humidified TDMA: Part II. Laboratory and ambient studies, *J. Atmos. Sci.*, *57*, 1872–1887.
- Buzorius, G., A. Zelenyuk, F. Brechtel, and D. Imre (2002), Simultaneous determination of individual ambient particle size, hygroscopicity and composition, *Geophys. Res. Lett.*, *29*(20), 1974, doi:10.1029/2001GL014221.
- Chan, M. N., and C. K. Chan (2003), Hygroscopic properties of two model humic-like substances and their mixtures with inorganics of atmospheric importance, *Environ. Sci. Technol.*, *37*, 5109–5115.
- Chan, M. N., and C. K. Chan (2005), Mass transfer effects in hygroscopic measurements of aerosol particles, *Atmos. Chem. Phys. Discuss.*, *5*, 4057–4082.
- Chan, M. N., and C. K. Chan (2007), Mass transfer effects on the hygroscopic growth of ammonium sulfate particles with a water-insoluble coating, *Atmos. Environ.*, *41*, 4423–4433.
- Charlson, R. J., and M. J. Pilat (1969), Climate: The influence of aerosols, *J. Appl. Meteorol.*, *8*, 1001–1002.
- Collaud Coen, M., E. Weingartner, S. Nyeki, J. Cozic, S. Henning, B. Verheggen, R. Gehrig, and U. Baltensperger (2007), Long-term trend analysis of aerosol parameters at the high-alpine site Jungfraujoch, *J. Geophys. Res.*, *112*, D13213, doi:10.1029/2006JD007995.
- Cziczo, D. J., D. S. Thomson, and D. M. Murphy (2001), Ablation, flux, and atmospheric implications of meteors inferred from stratospheric aerosol, *Science*, *291*, 1772–1775.
- DeMott, P. J., D. J. Cziczo, A. J. Prenni, D. M. Murphy, S. M. Kreidenweis, D. S. Thomson, R. Borys, and D. C. Rogers (2003), Measurements of the concentration and composition of nuclei for cirrus formation, *Proc. Natl. Acad. Sci.*, *100*, 14,655–14,660.

- Dessiatier, Y., T. Nguyen, T. Baer, and R. E. Miller (2003), IR vaporization mass spectrometry of aerosol particles with ionic solutions: The problem of ion-ion recombination, *J. Phys. Chem. A*, *107*, 11,245–11,252.
- Dinar, E., I. Taraniuk, E. R. Graber, T. Anttila, T. F. Mentel, and Y. Rudich (2007), Hygroscopic growth of atmospheric and model humic-like substances, *J. Geophys. Res.*, *112*, D05211, doi:10.1029/2006JD007442.
- Draxler, R., and G. Rolph (2003), Hysplit (hybrid single-particle lagrangian integrated trajectory), Website, NOAA Air Resources Laboratory, Silver Spring, MD. (Available at <http://www.arl.noaa.gov/ready/hysplit4.html>)
- Dusek, U., et al. (2006), Size matters more than chemistry for cloud-nucleating ability of aerosol particles, *Science*, *312*, 1375–1378.
- Forster, P., et al. (2007), Changes in atmospheric constituents and in radiative forcing, in *Climate Change*, Fourth Assessment Report of Working Group I of the Intergovernmental Panel on Climate Change, Cambridge University Press, U. K.
- Gard, E., J. E. Mayer, B. D. Morrical, R. Dienes, D. P. Fergenson, and K. A. Prather (1997), Real-time analysis of individual atmospheric aerosol particles: Design and performance of a portable ATOFMS, *Anal. Chem.*, *69*, 4083–4091.
- Gard, E., et al. (1998), Direct observation of heterogeneous chemistry in the atmosphere, *Science*, *279*, 1184–1187.
- Gross, D. S., M. E. Gälli, P. J. Silva, and K. A. Prather (2000), Relative sensitivity factors for alkali metal and ammonium cations in single-particle aerosol time-of-flight mass spectra, *Anal. Chem.*, *72*, 416–422.
- Gross, D. S., A. R. Barron, E. M. Sukovich, B. S. Warren, J. C. Jarvis, D. T. Suess, and K. A. Prather (2005), Stability of single particle tracers for differentiating between heavy- and light-duty vehicle emissions, *Atmos. Environ.*, *39*(16), 2889–2901.
- Gross, D. S., J. J. Schauer, L. Chen, R. Ramakrishnan, A. Ritz, T. Smith, and D. R. Musicant (2006), Enchilada: A Data-Mining Application for the Analysis of Atmospheric Mass Spectrometry Data, Poster presentation and published abstract, International Aerosol Conference, St. Paul, MN, USA.
- Gysel, M., E. Weingartner, S. Nyeki, D. Paulsen, U. Baltensperger, I. Galambos, and G. Kiss (2004), Hygroscopic properties of water-soluble matter and humic-like organics in atmospheric fine aerosol, *Atmos. Chem. Phys.*, *4*(1), 35–50.
- Hansson, H. C., A. Wiedensohler, M. J. Rood, and D. S. Covert (1990), Experimental determination of the hygroscopic properties of organically coated aerosol particles, *J. Aerosol. Sci.*, *21*, S241–S244.
- Hegg, D. A., D. S. Covert, K. K. Crahan, H. H. Jonsson, and Y. Liu (2006), Measurements of aerosol size-resolved hygroscopicity at sub and supermicron sizes, *Geophys. Res. Lett.*, *33*, L21808, doi:10.1029/2006GL026747.
- Henning, S., E. Weingartner, M. Schwikowski, H. W. Gäggeler, R. Gehrige, K.-P. Hinz, A. Trimborn, B. Spengler, and U. Baltensperger (2003), Seasonal variation of water-soluble ions of the aerosol at the high-alpine site Jungfraujoch (3580 m asl), *J. Geophys. Res.*, *108*(D1), 4030, doi:10.1029/2002JD002439.
- Holecck, J. C., M. T. Spencer, and K. A. Prather (2007), Analysis of rainwater samples: Comparison of single particle residues with ambient particle chemistry from the northeast Pacific and Indian oceans, *J. Geophys. Res.*, *112*, D22S24, doi:10.1029/2006JD008269.
- Hu, J. H., and J. P. D. Abbatt (1997), Reaction probabilities for N₂O₅ hydrolysis on sulfuric acid and ammonium sulfate aerosols at room temperature, *J. Phys. Chem.*, *101*, 871–878.
- Imhof, D., E. Weingartner, C. Ordóñez, R. Gehrige, M. Hill, B. Buchmann, and U. Baltensperger (2005), Real-world emission factors of fine and ultrafine aerosol particles for different traffic situations in Switzerland, *Environ. Sci. Technol.*, *39*, 8341–8350.
- IPCC (2007), *Climate Change 2007: The Physical Science Basis*. Contribution of Working Group I to the Fourth Assessment Report of the Intergovernmental Panel on Climate Change, Cambridge University Press, Cambridge, United Kingdom and New York, NY, USA.
- Johnson, K. S., B. Zuberi, L. T. Molina, M. J. Molina, M. J. Iedema, J. P. Cowin, D. J. Gaspar, C. Wang, and A. Laskin (2005), Processing of soot in an urban environment: Case study from the Mexico City metropolitan area, *Atmos. Chem. Phys.*, *5*(11), 3033–3043.
- Koehler, K. A., S. M. Kreidenweis, P. J. DeMott, A. J. Prenni, C. M. Carrico, B. Ervens, and G. Feingold (2005), Water activity and activation diameters from hygroscopicity data: Part II. Application to organic species, *Atmos. Chem. Phys.*, *6*, 795–809.
- Kreidenweis, S. M., K. Koehler, P. J. DeMott, A. J. Prenni, C. Carrico, and B. Ervens (2005), Water activity and activation diameters from hygroscopicity data: Part I. Theory and application to inorganic salts, *Atmos. Chem. Phys.*, *5*, 1357–1370.
- Lanz, V. A., et al. (2008), Source attribution of submicron organic aerosols during wintertime inversions by advanced factor analysis of aerosol mass spectra, *Environ. Sci. Technol.*, *42*, 214–220.
- Laskin, A., T. W. Wietsma, B. J. Krueger, and V. H. Grassian (2005), Heterogeneous chemistry of individual mineral dust particles with nitric acid: A combined CCSEM/EDX, ESEM, and ICP-MS study, *J. Geophys. Res.*, *110*, D10208, doi:10.1029/2004JD005206.
- Liu, P., P. J. Ziemann, D. B. Kittelson, and P. H. McMurry (1995a), Generating particle beams of controlled dimensions and divergence: I. Theory of particle motion in aerodynamic lenses and nozzle expansions, *Aerosol. Sci. Technol.*, *22*, 293–313.
- Liu, P., P. J. Ziemann, D. B. Kittelson, and P. H. McMurry (1995b), Generating particle beams of controlled dimensions and divergence: II. Experimental evaluation of particle motion in aerodynamic lenses and nozzle expansions, *Aerosol. Sci. Technol.*, *22*, 293–313.
- Lohmann, U., and J. Feichter (2005), Global indirect aerosol effects: A review, *Atmos. Chem. Phys.*, *5*, 715–737.
- Marcolli, C., and U. K. Krieger (2006), Phase changes during hygroscopic cycles of mixed organic/inorganic model systems of tropospheric aerosols, *J. Phys. Chem.*, *110*(5), 1881–1893.
- Marcolli, C., B. P. Luo, and T. Peter (2004), Mixing of the organic aerosol fractions: Liquids as the thermodynamically stable phases, *J. Phys. Chem.*, *108*(12), 2216–2224.
- McCormick, R. A., and J. H. Ludwig (1967), Climate modification by atmospheric aerosols, *Science*, *156*, 1358–1359.
- McMurry, P. H., M. Litchy, P. F. Huang, X. Cai, B. Turpin, W. D. Dick, and A. Hanson (1996), Elemental composition and morphology of individual particles separated by size and hygroscopicity with the TDMA, *Atmos. Environ.*, *30*, 101–108.
- Middlebrook, A. M., et al. (2003), A comparison of particle mass spectrometers during the 1999 Atlanta Supersite Project, *J. Geophys. Res.*, *108*(D7), 8424, doi:10.1029/2001JD000660.
- Mikhailov, E. F., S. S. Vlasenko, I. A. Podgorny, V. Ramanathan, and C. E. Corrigan (2006), Optical properties of soot-water drop agglomerates: An experimental study, *J. Geophys. Res.*, *111*, D07209, doi:10.1029/2005JD006389.
- Mozurkewich, M., and J. G. Calvert (1988), Reaction probability of N₂O₅ on aqueous aerosols, *J. Geophys. Res.*, *93*, 15,889–15,896.
- Murphy, D. M. (2007), The design of single particle laser mass spectrometers, *Mass Spectrom. Rev.*, *26*, 150–165.
- Murphy, D. M., and D. S. Thomson (1997a), Chemical composition of single aerosol particles at Idaho Hill: Negative ion measurements, *J. Geophys. Res.*, *102*(D5), 6353–6368.
- Murphy, D. M., and D. S. Thomson (1997b), Chemical composition of single aerosol particles at Idaho Hill: Positive ion measurements, *J. Geophys. Res.*, *102*(D5), 6341–6352.
- Murphy, D. M., D. J. Cziczo, K. D. Froyd, P. K. Hudson, B. M. Matthew, A. M. Middlebrook, R. E. Peltier, A. Sullivan, D. S. Thomson, and R. L. Weber (2006), Single-particle mass spectrometry of tropospheric aerosol particles, *J. Geophys. Res.*, *111*, D23S32, doi:10.1029/2006JD007340.
- Nenes, A., R. J. Charlson, M. C. Facchini, M. Kulmala, A. Laaksonen, and J. H. Seinfeld (2002), Can chemical effects on cloud droplet number rival the first indirect effect?, *Geophys. Res. Lett.*, *29*(17), 1848, doi:10.1029/2002GL015295.
- Petters, M. D., A. J. Prenni, S. M. Kreidenweis, P. J. DeMott, A. Matsunaga, Y. B. Lim, and P. J. Ziemann (2006), Chemical aging and the hydrophobic-to-hydrophilic conversion of carbonaceous aerosol, *Geophys. Res. Lett.*, *33*, L24806, doi:10.1029/2006GL027249.
- Pitchford, M., and P. McMurry (1994), Relationship between measured water vapor growth and chemistry of atmospheric aerosol for Grand Canyon, Arizona, in winter, 1990, *Atmos. Environ.*, *28*, 827–840.
- Rader, D., P. McMurry, and S. Smith (1987), Evaporation rates of monodisperse organic aerosols in the 0.02- to 0.2-mm-diameter range, *Aerosol. Sci. Technol.*, *6*, 247–260.
- Rosenfeld, D., and I. M. Lensky (1998), Satellite-based insights into precipitation formation processes in continental and maritime convective clouds, *Bull. Am. Met. Soc.*, *79*, 2457–2476.
- Seinfeld, J. H., and S. N. Pandis (2006), *Atmospheric Chemistry and Physics*, John Wiley & Sons, Hoboken, NJ.
- Sjogren, S., M. Gysel, E. Weingartner, M. R. Alfarra, J. Duplissy, J. Cozic, J. Crosier, H. Coe, and U. Baltensperger (2007), Hygroscopicity of the submicrometer aerosol at the high-alpine site Jungfraujoch, 3580 m a.s.l., Switzerland, *Atmos. Chem. Phys. Discuss.*, *7*, 13,699–13,732.
- Sullivan, R. C., and K. A. Prather (2005), Recent advances in our understanding of atmospheric chemistry and climate made possible by on-line aerosol analysis instrumentation, *Anal. Chem.*, *77*, 3861–3886.
- Svenningsson, B., et al. (2006), Hygroscopic growth and critical supersaturations for mixed aerosol particles of inorganic and organic compounds of atmospheric relevance, *Atmos. Chem. Phys.*, *6*, 1937–1952.
- Topping, D. O., G. B. McFiggans, and H. Coe (2005), A curved multi-component aerosol hygroscopicity model framework: Part 1. Inorganic compounds, *Atmos. Chem. Phys.*, *5*, 1205–1222.

- Twomey, S. (1977), The influence of pollution on the shortwave albedo of clouds, *J. Atmos. Sci.*, 34, 1149–1152.
- Weingartner, E., H. Burtscher, and U. Baltensperger (1997), Hygroscopic properties of carbon and diesel soot particles, *Atmos. Environ.*, 31, 2311–2327.
- Weingartner, E., S. Nyeki, and U. Baltensperger (1999), Seasonal and diurnal variation of aerosol size distributions ($10 < D < 750$ nm) at a high-alpine site (Jungfraujoch 3580 m asl), *J. Geophys. Res.*, 104, 26,809–26,820.
- Weingartner, E., M. Gysel, and U. Baltensperger (2002), Hygroscopicity of aerosol particles at low temperatures: 1. New low-temperature h-tdma instrument: Setup and first applications, *Environ. Sci. Technol.*, 36, 55–62.
- Weiss, M., P. J. T. Verheijen, J. C. M. Marijnissen, and B. Scarlett (1997), On the performance of an on-line time-of-flight mass spectrometer for aerosols, *J. Aerosol. Sci.*, 28, 159–171.
- Wenzel, R. J., D.-Y. Liu, E. S. Edgerton, and K. A. Prather (2003), Aerosol time-of-flight mass spectrometry during the Atlanta Supersite Experiment: 2. Scaling procedures, 108(D7), 8427, *J. Geophys. Res.*, doi:10.1029/2001JD001563.
- Zelenyuk, A., D. Imre, and L. A. Cuadra-Rodriguez (2006), Evaporation of water from particles in the aerodynamic lens inlet: An experimental study, *Anal. Chem.*, 78, 6942–6947.
-
- U. Baltensperger, M. Gysel, L. Kammermann, and E. Weingartner, Laboratory of Atmospheric 880 Chemistry, Paul Scherrer Institut, CH-5232 Villigen PSI, Switzerland.
- D. J. Cziczo, Atmospheric Science and Global Change, Pacific Northwest National Laboratory, MSIN K9-24, Richland, WA 99354, USA. (daniel.cziczo@pnl.gov)
- H. Herich and U. Lohmann, Institute for Atmospheric and Climate Science, ETH Zurich, Universitaetsstrasse 16, CH-8093 Zurich, Switzerland.